HHS Public Access

Author manuscript

Small. Author manuscript; available in PMC 2023 September 01.

Published in final edited form as:

Small. 2022 September ; 18(38): e2202694. doi:10.1002/smll.202202694.

Reactive oxygen species responsive cleavable hierarchical metallic supra-nanostructure

Hyunjun Choi[+],
Department of Radiology, Feinberg School of Medicine, Northwestern University, Chicago, IL 60611, USA

Department of Biomedical Engineering, University of Illinois at Chicago, Chicago, IL 60607, USA

Bongseo Choi[+],
Department of Radiology, Feinberg School of Medicine, Northwestern University, Chicago, IL 60611, USA

Jun-Hyeok Han,
Department of Biomedical-Chemical Engineering, The Catholic University of Korea, 43 Jibong-ro, Bucheon, Gyeonggi 14662, Republic of Korea

Department of Biotechnology, The Catholic University of Korea, 43 Jibong-ro, Bucheon, Gyeonggi 14662, Republic of Korea

Ha Eun Shin,
Department of Biomedical-Chemical Engineering, The Catholic University of Korea, 43 Jibong-ro, Bucheon, Gyeonggi 14662, Republic of Korea

Department of Biotechnology, The Catholic University of Korea, 43 Jibong-ro, Bucheon, Gyeonggi 14662, Republic of Korea

Wooram Park,
Department of Biomedical-Chemical Engineering, The Catholic University of Korea, 43 Jibong-ro, Bucheon, Gyeonggi 14662, Republic of Korea

Department of Biotechnology, The Catholic University of Korea, 43 Jibong-ro, Bucheon, Gyeonggi 14662, Republic of Korea

Dong-Hyun Kim[*]
Department of Radiology, Feinberg School of Medicine, Northwestern University, Chicago, IL 60611, USA

Department of Biomedical Engineering, University of Illinois at Chicago, Chicago, IL 60607, USA

Department of Biomedical Engineering, McCormick School of Engineering, Evanston, IL 60208, USA

[*]Corresponding author: Prof. Dong-Hyun Kim, dhkim@northwestern.edu.
[+]H.C. and B.C. contributed equally to this work.

Conflict of Interest
The authors declare no conflict of interest.

Supporting Information
Supporting Information is available from the Wiley Online Library or from the author.

Robert H. Lurie Comprehensive Cancer Center, Chicago, IL 60611, USA

Abstract

We report a reactive oxygen species (ROS) responsive cleavable hierarchical metallic supra-nanostructure (HMSN). HMSN structured with thin branches composed by primary gold (Au) nanocrystals and silver (Ag) nano-linkers was synthesized by a one-pot aqueous synthesis with a selected ratio of Au/Ag/cholate. ROS responsive degradability of HMSN was tested in the presence of endogenous and exogeneous ROS. Significant ROS responsive structural deformation of HMSN was observed in the ROS exposure with hydrogen peroxide (H_2O_2) solution. The ROS responsiveness of HMSN was significantly comparable with negligible structural changes of conventional spherical gold nanoparticles. Demonstrated ROS responsive degradation of HMSN was further confirmed in various *in vitro* ROS conditions of each cellular endogenous ROS and exogeneous ROS generated by photodynamic therapy (PDT) or X-ray radiation. Then, *in vivo* ROS responsive degradability of HMSN was further evaluated with intratumoral injection of HMSN and exogeneous ROS generation via PDT in a mice tumor model. Additional *in vivo* biodistribution and toxicity of intravenously administrated HMSN at 30-day post injection were investigated for potential *in vivo* applications. Observed ROS responsive degradability of HMSN will provide a promising option for a type of ROS responsive-multifunctional nanocarriers in the cancer treatment and various biomedical applications.

Graphical Abstract

Here we found that hierarchical metallic supra-nanostructure (HMSN) composed by primary Au nanobranches connected with Ag nano-linkers was cleavable in the response to a biological endogenous reactive oxygen species (ROS) and exogeneous ROS condition. As given challenges of non-degradable and non-stimuli responsiveness of various potent inorganic nanoparticles, the introduction of ROS responsive cleavable HMSN suggests an exciting opportunity for the ROS-responsive nanocarrier applications.

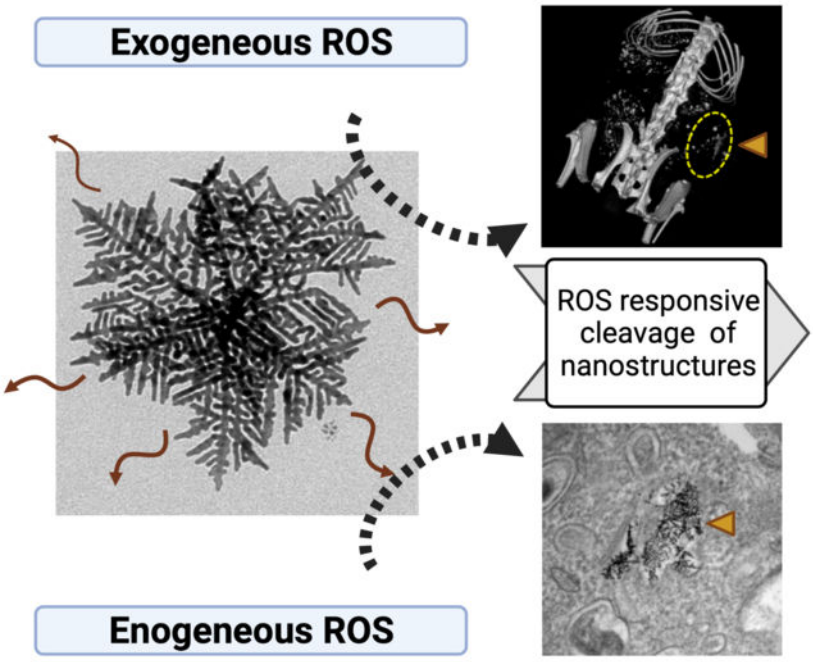

Keywords

reactive oxygen species; degradable nanostructure; gold nanoparticles; cancer therapy; degradable metal nanoparticles

1. Introduction

Cancer cells are representing deregulated redox homeostasis.[1] Tumor growth and malignant progression in high metabolic rate are induced with enhanced reactive oxygen species (ROS) level and an increased antioxidant ability.[1, 2] Cancer cell cycle arrest, senescence, and apoptosis are all associated with ROS.[3] ROS mediated cancer cell therapy such as photodynamic therapy (PDT) based therapies[4] or radiation therapies[5] that can alter redox homeostasis has considered a promising approach to suppress tumor burdens. Thus, the development of ROS responsive nanocarriers has been emerged as one of the impactive area in cancer medicine.[6, 7] Both of exogenously generated ROS or endogenous ROS in the tumor microenvironment (TME) are the effective sources for ROS responsive nanocarriers. Up to now, various ROS responsive organic ligands and polymer materials employing ROS responsive moieties have been investigated and utilized for ROS responsive cancer therapeutic applications.[8–10] Recently, multifunctional ROS responsive nanocarriers which can perform therapeutic/imaging in a single platform have been paid much attention as a promising form of ROS responsive nanocarriers.[11, 12] Hybrid organic/inorganic nanocarriers integrating ROS responsive moiety and multifunctional inorganic nanoparticles have been suggested for a type of multifunctional ROS responsive nanocarriers.[13, 14] However, combining multiple functions into one carrier system remains a challenge and limits their broad cancer therapy applications. In

addition, non-degradable inorganic nanoparticles in the hybrid platforms may induce side effect with low level of clearance. An effective ROS responsive degradable nanoparticle may be beneficial for the ROS triggered cancer therapeutics that can result in an enhanced treatment outcome with reduced side effects.

Here, we report a ROS responsive cleavable hierarchical metallic supra-nanostructure (HMSN). Anisotropic 2-dimensional (2D) HMSN composed by thin branches with primary gold (Au) nanocrystals and silver (Ag) nano-linkers was synthesized by the aqueous one-pot synthesis with a selected ratio of Au/Ag and sodium cholate, as we demonstrated in previous report.[15–17] The characterized HMSN structure was easily cleavable in various ROS conditions. Firstly, we observed that a ROS exposure to HMSN with a H_2O_2 solution dissociated the initial HMSN structure into ultra-small nanoparticles (~3 nm) that was comparable with negligible structural change of conventional spherical gold nanoparticles (SGNP). An effective ROS responsive structural degradation of HMSN was also demonstrated in both endogenous ROS in macrophage cells and exogeneous ROS generation by PDT or X-ray radiation. Finally, *in vivo* ROS responsive degradability of HMSN was evaluated with intratumoral injection of HMSN and exogeneous ROS treatment via PDT in A20 xenograft tumor model. Additional *in vivo* biodistribution and toxicity of intravenously administrated HMSN at 30-day post injection were investigated for potential clearance *in vivo* applications. The synthesized HMSN and their demonstrated *in vitro* and *in vivo* ROS responsive degradability provide a promising option for a type of ROS responsive-multifunctional nanocarriers in the cancer treatment and various biomedical applications. As given current challenges in clinical translation of non-degradable Au based metallic inorganic nanocarriers, the ROS responsive cleavable hierarchical multi-branched Au nanocarriers will provide an opportunity of ROS responsive nanocarriers and Au nanoparticles-based cancer nanomedicine.

2. Result and Discussion

2.1. Synthesis of HMSN and ROS responsive structural degradation

In our previous studies[15, 16, 18], we synthesized hierarchical Au supra-nanostructures using metal-cholate complexes. Silver halide nanocrystals (AgCl) in the metal-cholate nanocomplexes were rapidly formed after the mixing of $HAuCl_4{\cdot}3H_2O$ and $AgNO_3$ in cholate solution. Thereby the nanocomplexes concentrate both Au ions and AgCl nanoparticles inside cholate micelles. Subsequent addition of ascorbic acid reduced both Au ions and AgCl that eventually generated multibranched hierarchical Au supra-nanostructures. The branches were composed by randomly interconnected the primary Au nanoparticles with small Ag nanocrystals (< 3 nm). The final morphologies of hierarchically branched supra-nanostructures were controlled by the Au/Ag feed ratio. Herein HMSN was synthesized with the mixture of 5:1 molar ratio of $HAuCl_4{\cdot}3H_2O$ and $AgNO_3$ in the 1.8 mM sodium cholate solution and 100 mM of l-ascorbic acid for the potential ROS responsive cleavable Au nanocarriers (Figure 1a and S1a). The preferential Au crystal growth in the structure of cholate formed the HMSN which was composed with multi-straight branches including ~5.5 nm thickness major branches and ~4.4 nm thickness secondary branches (Figure 1a).[15] Hydrodynamic size of HMSN was about 200 nm (Figure 1b).

Unique alternating Au and Ag nanocrystal structure of HMSN allowed a significant structural deformation in the response to various H_2O_2 concentration. As shown in the DLS size distribution data of HMSN incubated in H_2O_2 solution for 7 days (Figure 1c), the increase of H_2O_2 concentration induced the decrease of average size of HMSN from 197 nm to 96 nm. At the same time, the new peaks in the size distribution were appeared after the exposure to ROS of H_2O_2 solutions. Relatively low 0.1 mM H_2O_2 concentration generated 25.3 nm of the 2nd peak. As the concentration of H_2O_2 increased to 1 M, 6.4 nm of 2nd peak was observed. These results indicated ROS responsive cleavage of HMSN resulting in small nanoparticles appearance. Resulted ROS responsive structural change of HMSN was further confirmed with morphology change dependent on ROS exposure time. TEM data showed that an intact HMSN structure before the ROS exposure was significantly deformed within 1-day of ROS exposure with 0.1 M of H_2O_2. After 4 weeks of the ROS exposure, the outer part of HMSN was remarkably dissociated to be smaller sized nanostructures (Figure 1d, 1e, and Figure S1b). About ~3.8 nm small nanoparticles cleaved from HMSN were primarily found in TEM images (Figure 1f). On the other hand, the 30-nm spherical gold nanoparticles showed no significant deformation during 4 weeks of ROS exposure. (Figure S2).

To further investigate the ROS responsive cleavage of HMSN, spatial distribution of Au and Ag elements in HMSN was measured with STEM. The STEM image of HMSN showed unique alternating Au and Ag nanostructures (Figure 2a and S3).[15] Inductively coupled plasma-mass spectrometry (ICP-MS) analysis indicated that the Au and Ag ratio of HMSN was 10.6:1. STEM images showed clear primary Au components (red) and secondary Ag components (green) of HMSN. However, the ROS exposure to the HMSN gradually leached out Ag components with the structural dissociation (Figure 2a). As shown in Ag/Au elemental intensity ratio, the Ag elemental intensity was significantly decreased at 4-day and 4-week post ROS treatment with H_2O_2 (Figure 2b). This result was further confirmed by measuring the released Ag component from HMSN with ICP-MS. A time dependent ROS responsive Ag release profile from HMSN showed 12 % of Ag leaching of HMSN for 72 hours co-incubation with 0.1 M H_2O_2 solution (Figure 2c). Additional STEM data showed that the remained HMSN structure after the ROS exposure was mainly composed by Au element with minor silver components (Figure S4). These all results indicate that HMSN branched structure composed by primary Au nanocrystals and Ag nano-linkers can be degradable with the selective ROS mediated etching of small Ag nanocrystal located between Au nanocrystals in HMSN (Figure 2d). Relatively lower reduction potential of Ag component (E=0.80 V) in the Au nanocrystal (E=1.50 V) allowed the preferential ROS mediated Ag etching in the H_2O_2 solution.[19] At the same time, galvanic replacement between Au and Ag can occur in the presence of H_2O_2 for the selective sacrifice of small Ag nano-linkers.[20–23] Consequently, the structural deformation and degradation of HMSN was induced due to the selective dissolution of Ag nano-linkers in the presence of ROS.

2.2. In vitro cellular endogenous ROS responsive cleavage of HMSN

Demonstrated ROS responsive structural deformation with H_2O_2 solution was further studied for intracellular ROS responsiveness of HMSN using RAW 264.7 macrophage cells. HMSN was incubated with RAW 264.7 macrophage cells and their intracellular ROS responsive degradation was compared with a conventional spherical gold nanoparticle

(SGNP) in confocal fluorescent microscope, confocal reflective microscope, and cell TEM images. As shown in Figure 3a, HMSN taken up by macrophage cells was clearly visible with black dots in confocal microscopic images at 1 day of post-incubation, as similar with SGNP treated cells. Those black dots indicating HMSN in cells were removed at 7-day post-treatment, while those SGNP treated cells still showed agglomerated nanoparticles. Dark field images of the cells also confirmed the significant signal reduction of HMSN at 7-day incubation (Figure 3b). Intense and bright contrast of HMSN in cells at 1 day incubation was decreased and diluted at 7-day incubation period. However, the concentrated bright signal of SGNP was still visible in 7-day incubation. The significant exclusion of HMSN might be induced by intracellular ROS in the macrophages. The macrophages are phagocytes that can respond to nanoparticles by uptake and production of large quantity of ROS by respiratory burst[24, 25] to neutralize and digest nanoparticles in phagosomes or lysosomes.[26–28] As shown in cellular ROS imaging of macrophages, each nanoparticles treatment significantly enhanced the ROS level in the cells. At 1-day post-treatment, strong ROS signals were observed in both HMSN and SGNP treated cells. Then, the cells incubated with HMSN showed a significant ROS decrease from 2-day incubation. On 7-day incubation of HMSN, the cellular ROS level was dropped down to the similar with the ROS level of control group (Figure 3c and 3d). When a ROS inhibitor, N-acetyl cysteine, was treated in the cells, the clearance of HMSN was also inhibited. The reflectance signal from cells treated with HMSN was not decreased by the time up to 7 days, indicating that the cells could not digest HMSN in the inhibited cellular ROS generation (Figure S5). It is indicating that the intracellular endogenous ROS allowed the degradation of HMSN. Finally, the intracellular ROS cleavage of HMSN was further confirmed with TEM images of the cells incubated with HMSN. As shown in Figure 3e, the branched structure of HMSN taken up by macrophages was significantly deformed to be dissociated into short branches in the hot ROS spots such as endosome or phagosome of cells.[22, 29] Longer incubation of HMSN with macrophage cells progressed the cleavage of HMSN, resulting the presence of smaller nano-fragments in intracellular vesicles corresponding to lysosome, or endosome, multivesicular bodies.

Although those significant removal of HMSN in the confocal microscope images can be involved exocytosis or physical exclusion, the significant size decrease and morphology change of HMSN in the intracellular vesicles might prove the endogenous ROS responsive cleavage and removal of HMSN. Taken together those cellular interaction data of HMSN, HMSN can be cleavable and degraded with the intracellular endogenous ROS, as demonstrated ROS responsive HMSN degradation in the H_2O_2 solution.

2.3. Exogeneous ROS responsive degradability of HMSN

ROS responsive degradable HMSN can have great potential for various ROS mediated therapeutic applications such as PDT and radiation therapies. Next, therapeutic mediated exogenous ROS responsive degradability of HMSN was demonstrated with well-established PDT using Ce6 photosensitizers and X-ray radiation, respectively. As shown in Figure 4a, PDT mediated exogenous ROS significantly cleaved the branches of HMSN in the aqueous solution. The average size of HMSN (about 206 nm) was significantly decreased to 137 nm in the ROS exposure time dependent manner (Figure 4b). The ROS mediated degradation

of HMSN was further confirmed in a tissue phantom (1 % agarose gel) mimicking a tissue environment. PDT mediated ROS was applied to HMSN implanted in tissue phantoms (Figure 4c). Injected HMSN in the center of phantoms after 70 hours of PDT treatment was diffused 3-folds further distance from the injection center than non-ROS treated group. It is indicating the ROS responsive cleaved small branches of HMSN travels further with less hinderance in the gel network compared to non-ROS treated HMSN (Figure 4d and e).[30] Subsequently, PDT mediated exogenous ROS responsive structural deformation and degradability of HMSN was tested *in vivo* with BALB/c mice bearing subcutaneously inoculated A20 tumor (Figure 4f). HMSN with Ce6 was successfully injected into the center of tumor with innate CT contrast effect of HMSN (21 HU/mg/mL, Figure S6) in CT scanning (Figure 4f).[15, 16] Then, ROS was generated with the non-thermal laser (652 nm) for 30 mins. The distribution of injected HMSN in the tumor was measured with CT contrast change at 1-day post ROS treatment (Figure 4f and 4g). PDT-ROS treated HMSN showed a significant reduction of CT contrast intensity (Figure 4f and S7). However, PDT-ROS treated SGNP showed no significant diffusion or reduction of CT contrast (Figure S7). The demonstrated exogenous ROS responsive cleavage and degradability of HMSN may have a potential role for the combinational ROS mediated cancer therapeutic applications utilizing established cancer therapies such as PDT or radiation therapies (Figure S8).[18, 31, 32]

2.4. In vivo biodistribution of intravenously injected ROS responsive degradable HMSN

ROS responsive degradation of HMSN can be useful for the clearance of nanocarriers as well as local ROS triggered delivery of therapeutics. As shown endogenous ROS responsive degradation of HMSN, IV injected HMSN can have enhanced clearance property compared to conventional non-degradable inorganic nanoparticles. As previously reported, the majority of the injected nanocarriers is cleared by cells such as macrophages in blood circulation and accumulated in the mononuclear phagocyte system (MPS) including the liver and spleen.[33] The accumulated nanocarriers are going through ROS mediated digestion and the renal/biliary clearance. We hypothesized that our ROS responsive degradable HMSN can show faster clearance compared to conventional SGNP. Here, the biodistribution of IV injected HMSN was measured with Au elemental quantification in organs at 3-day and 30-day post injection and compared with the biodistribution of SGNP in C57BL/6 mice (Figure 5). The quantification of Au element in each organ showed that IV injected HMSN was primarily accumulated in the liver and spleen as well as SGNP. However, the relative accumulation of HMSN in kidney (Ki), small intestine (SI) and large intestine (LI) was significantly higher than the mice treated with SGNP. This result might indicate the IV injected HMSN was degraded in the liver into smaller particles and secreted by hepatobiliary pathway than non-ROS responsive SGNP.[34] Also, degraded small nanoparticles from HMSN may diffuse out from the organ and travel back to circulation. It is supported by the accumulation of Au in the kidney and the constant presence of Au element detected in blood (0.016 %ID/g at 3 days and 0.018 %ID/g 30 days post injection) throughout a month while the Au element was not detected in case of the mice treated with SGNP at 30 days post injection (Figure 5b). Furthermore, at 30 days post injection, the liver and spleen accumulation of HMSN was decreased from the initial detected accumulations at 3 days post injection. On the contrary, SGNP injected mice showed no change of the Au accumulation in the liver and spleen. Also, SGNP injected mice did not show significant Au accumulation

in their excretory organs (Figure 5a). There are numerous distributional studies of SGNP, demonstrating the retention time of non-degradable SGNP *in vivo* may be extremely long more than a year without major deformation of nanoparticles.[35, 36] However, our ROS responsive degradable HMSN might have the faster clearance property as shown in the biodistribution data. Although more systemic investigation about the clearance of HMSN is required, our preliminary biodistribution data indicated potential renal clearance property of HMSN that can mitigate long-term toxicity of the materials.

Although *in vitro* cytotoxicity assay of HMSN in Clone-9 hepatocytes showed no significant toxicity in a concentration range up to 250 μg/mL of HMSN (Figure S9), *in vivo* safety of ROS responsive nanocarriers is a critical component for the potential *in vivo* applications. In the biodistribution analysis, *in vivo* toxicity of HMSN was investigated together. During the treatment period by 30-day, the body weights of the mice treated with the nanoparticles had no appreciable change. No obvious histopathological abnormalities were found in these tissue sections at 7-day and 30-day, suggesting negligible adverse toxicity of HMSN (Figure 5c). H&E histology data of organs from the mice treated with IV injection of 100 μg HMSN or SGNP at 3-day and 30-day post-injection showed no severe toxicity caused by injected nanoparticles in organs related to reticuloendothelial and excretory system. In kidney, focal and segmental glomerulosclerosis warning the renal toxicity was not found in kidney sections, and liver sections showed well-integrated structure of portal triad. Plus, there was no neutrophil infiltration and formation of foreign body giant cells in liver, and there was no significant geminal center maturation in spleen after treatment of HMSN compared to PBS treated control. The examination of the hematology values of mice treated with nanoparticles provided the information about potential liver- and kidney-function impairment. Compared to the control group, no significant changes in hematological parameters were found in HMSN injected animals as well as SGNP in our dosage (Figure S10). There were no significant changes in AST and ALT, key markers of liver injury, on day 7-day post injection of HMSN and SGNP injection.

3. Conclusion

ROS responsive nanocarriers have been structured with the addition of various ROS responsive functional groups or linkers to the polymeric nanocarriers or multifunctional inorganic nanocarriers. However, combining of the independently developed ROS sensitive moieties and nanoparticles carriers as a single platform can be challenging to extend their broad cancer therapy applications. In our study, HMSN structured with thin Au branches connected with Ag nano-linkers was synthesized. The ROS responsive cleavage of HMSN was demonstrated in various biological ROS conditions. Here we found that Ag nano-linkers in widely exposed thin Au branches of HMSN was selectively removed in the response to a biological endogenous ROS and therapeutic exogeneous ROS condition. Due to well-known superior optical properties and catalytic activity of branched Au nanoparticles that can be utilized for sensing, imaging agents, and therapeutics and so on over spherical Au nanoparticles, HMSN could be a promising option for the ROS-responsive multifunctional nanocarriers. As given current challenges of non-degradable character and non-stimuli responsiveness of various potent inorganic nanoparticles for *in vivo* ROS-responsive nanocarrier applications, the introduction of ROS responsive cleavable HMSN suggests

an exciting opportunity of the use of multifunctional inorganic nanoparticles for the ROS-responsive nanocarrier applications. Further, considering the impact of ROS biology, cellular oxidative stress, and ROS mediated therapeutics, ROS responsive cleavable HMSN provides a promising option for targeted drug delivery, localized combination immunotherapy, peroxidase-like nanozymes, sensors, and advanced ROS related medical applications.

4. Experimental Section

4.1. Materials

Gold(III) chloride trihydrate, silver nitrate, l-ascorbic acid, sodium cholate hydrate, Gold nanoparticle standard suspension (200 nm), Milli-Q grade water, HS-PEG3500-COOH, HS-PEG3500-NH2, sodium citrate, 30 % v/v hydrogen peroxide solution, Chlorine e6 (Ce6), N-(3-Dimethylaminopropyl)-N'-ethylcarbodiimide hydrochloride (EDC), N-hydroxysuccinimide (NHS), N-acetyl cysteine (NAC), and agarose were purchased from Sigma-Aldrich (Saint Louis, MO, USA). Chlorine e6 (Ce6) was purchased from Frontier Scientific (Logan, UT, USA).

4.2. Synthesis of HMSN

The synthetic protocol was modified from the previous paper we published.[15, 16, 18] Briefly, 10 mL of 1.8 mM sodium cholate solution was prepared in glass vial and stirred at 350 rpm. Then, 1 mL of 5 mM $HAuCl_4 \cdot 3H_2O$ and 100 μL of 10 mM $AgNO_3$ solution was subsequently added into 20 second interval. 150 μL of 100 mM l-ascorbic acid was added into reaction mixture and incubated for 20 second strictly at 350 rpm. Finally, the reaction mixture was left without agitation for 4 hours, and 100 μL of 100 mg/mL thiol-PEG-carboxylate was added to reaction mixture. The nanoparticle suspension was incubated for 12 hours. For purification, suspension of HMSN was centrifugated at 6500 rpm for 30 minutes, and supernatant solution was discarded. The purification step was repeated for 5 times. 30-nm spherical gold nanoparticles (SGNP) were synthesized with Turvekich method, and citrate groups on the surface of SGNP was replaced with thiol-PEG carboxylate. The synthesized HMSN was observed in transmission electron microscope (TEM) for demonstration of structure and was measured by dynamic light spectroscopy (DLS) for determination of size information. Quantification of gold and silver element in HMSN was measured with ICP-MS, and the elemental distribution in nanoparticles was acquired by EDS function with STEM.

4.3. Demonstration of ROS responsive degradability of HMSN in H_2O_2

1 mL of HMSN suspension (100 μg/mL) or same volume of SGNP (30 nm) were loaded in dialysis membrane (MW cut: 10 kD), and the membrane was incubated in H_2O_2 solution with various concentration (0, 0.1, 1, 100, and 1000 mM) for up to 4 weeks in 37 °C. To maintain the initial concentration of H_2O_2 exposing to gold nanoparticles, the media outside of dialysis membrane was replaced with H_2O_2 solution freshly prepared from 30 %v/v H_2O_2 stock solution. After the incubation, the suspension containing gold nanoparticles in dialysis membrane was collected and measured with TEM and DLS for morphological analysis and size determination, respectively. The elemental distribution of nanoparticles in the samples incubated in H_2O_2 solution was measured with STEM in predetermined time

points (control, 4 days, 4 weeks). For quantification of silver ions released from HMSN during co-incubation with ROS source, 100 μL of 25 mg/mL HMSN suspension was added into centrifugal tube containing 900 μL of 0.1 M H_2O_2. Hence, at predetermined time points, sample solutions were centrifugated using Amicon Ultra centrifugal filter (100 kD) (Millipore, MA, USA). The filtered solution was weighed and treated with trace metal grade nitric acid and hydrogen peroxide for ICP-MS analysis. The silver element in sample solution was measured using ICP-MS.

4.4. In vitro intracellular endogenous ROS responsive degradability of HMSN

RAW 264.7 macrophage cell line was used for the in vitro experiments. 4000 cells in 2 mL of media containing samples (non-treated, 10 μg/mL of HMSN, 10 μg/mL of SGNP (30 nm)) were seeded in culture dishes for confocal microscopy and incubated up to 7 days. For ROS generation in macrophages, after the incubation with nanoparticles in predetermined time (1, 2, 4, and 7 days), the media was discarded and replaced with the media containing 5 μM DCF2DA. After 40 minutes of incubation in incubation chamber, the cells were imaged by confocal microscope with excitation / emission at 485 nm / 535 nm. For confocal reflectance microscopy, living macrophage cells in confocal dish were directly imaged by reflectance microscope (Nikon A1R) equipped with O_2 and CO_2 chamber. To determine the effect of ROS on degradation of HMSN, the group with treatment of N-acetyl cysteine (NAC) as a ROS inhibitor (4 mM) was tested. Macrophage cells were incubated with HMSN for 14 days, fixed with formaldehyde and glutaraldehyde solution, and centrifugated at 1500 rpm for 5 minutes. The supernatant was discarded and 200 μL of 3 % agarose was added to the pellet and mixed gently. The block was dehydrated with ethanol (50, 75, 90, and 100 % v/v) and sectioned with ultramicrotome for obtaining TEM sections. After the placement of sections on TEM grids, the cells and intracellular structures were measured by TEM.

4.5. ROS therapeutic mediated exogenous ROS responsive degradability of HMSN

For testing the exogenous ROS responsive degradability of HMSN, 500 μL of 10 μg/mL Ce6 (photosensitizer) was mixed with the suspension containing 500 μL of 100 μg/mL HMSN. Then, 652 nm wavelength laser was irradiated up to dosage of 450 J/cm^2 to sample in a dark room. Samples were collected after the treatment of various laser exposure condition at 150, 350, and 450 J/cm^2, and measured with TEM and DLS. X-ray irradiation was also tested for the exogenous ROS responsive degradability of HMSN, 100 μg/mL HMSN in Milli-Q grade water was irradiated with X-ray (up to 100 Gy), and samples were taken for TEM and DLS measurement to observe morphological changes and hydrodynamic size change respectively after ROS treatments.

4.6. Exogenous ROS responsive degradability of HMSN in artificial tissue phantom

Ce6 conjugated HMSN was synthesized with EDC/NHS conjugation method. Briefly, 2.4 mg of HMSN was resuspended with Amine-PEG-thiol (MW: 3500). 0.2 mg of Ce6 dissolved in 5 mL of DMSO was treated with 5 mg of EDC and 3 mg of NHS. Then, the mixture was mixed with gold suspension and incubated in a dark room at room temperature for 8 hours. Ce6 conjugated HMSN was purified with dialysis and centrifugation for further use. 1 % w/v agarose gel was prepared in 6 well plates, and 5 μL of Ce6 conjugated HMSN (2 mg/mL) was seeded in the center of gel. The gel was treated with 652 nm laser (450

J/cm^2) and the diffusivity of nanoparticle in gel was imaged with digital camera (ILCE-7C, Sony, Japan). The images were processed with threshold function of ImageJ software, and the average distance of nanoparticle diffusion from the seeded point was measured.

4.7. In vivo exogenous ROS responsive degradability of HMSN in tumor

All animal experiments were approved by institutional IACUC (Protocol number: IS00002377). Female BALB/c mice were used to test the enhanced diffusivity of nanoparticles by treatment of ROS induction by a photosensitizer (Ce6) and irradiation of 652-nm laser in vivo. 1×10^6 cells of A20 (B cell lymphoma) cell line were inoculated subcutaneously near thigh of mice. After the tumor size reached to diameter of 1 cm, the 10 mg/kg of Ce6 and 500 μg of HMSN or spherical gold nanoparticle (200 nm) were injected by intratumoral route. Then, 150 J/cm^2 of laser dose (652 nm) was treated on tumor. Each step was imaged with MicroCT (35 kV, 450 ms, NanoScan PET/CT, Mediso, USA) for evaluation of gold distribution in the tumors. The acquired DICOM scans were processed with Radiant Viewer (Medixant, Poland) to reconstruct 3-dimensional body images. The distribution of CT contrast among sections were analyzed by following methods. Firstly, maximum contrast effect (HU) of transverse CT sections were measured by elliptical method with the area of 0.03 cm^2. After all maximum values in selected area in each slice were obtained, the slice that showed highest maximum intensity by gold nanoparticles in tumor was positioned at zero, and the slices directed to cranial position were counted negatively (−), and the slices directed to caudal position were counted positively (+).

4.8. Biodistribution and histological analysis, hematological response of IV injected ROS responsive degradable HMSN

All animal experiments were approved by institutional IACUC (Protocol number: IS00002377). 100 μg of nanoparticle suspensions (HMSN or SGNP (30 nm)) was intravenously injected via tail vein of C57BL/6 mice. The mice were sacrificed at predetermined time points, and organs were collected for biodistribution assay. The collected organs were digested with nitric acid and hydrogen peroxide at 70°C for 12 hours. The gold in digested organ solution was dissolved with hydrochloric acid. The mass of elemental gold in organs were measured using ICP-MS. Also, cell viability was measured using CCK-8 assay kit (Dojindo) to evaluate possible toxicity of HMSN. To evaluate the tissue viability and response to nanoparticles, Hematoxylin-Eosin staining was performed to the tissue 30 days after I.V administration of 100 μg of gold nanoparticles (HMSN or SGNP). To determine possible toxicity, the serum was isolated from the blood of mice treated with PBS, 50 μg of SGNP, and 50 μg of HMSN via I.V injection.

4.9. Statistical analysis

Analysis results were presented as mean ± standard deviation (S.D) or poly dispersity index (PDI). For statistical evaluation, All experiments are performed at least 3 times independently. The nanoparticle samples were triplicated for the tests including ROS incubation tests, in vitro tests, X-ray and PDT tests, and HMSN diffusivity tests in phantom agarose gel. Mean fluorescence intensity was averaged after the quantification of ROI with imageJ from the selection of 100 cells in confocal microscopic images. For in vivo

experiments, 5 mice for each of the groups were used for the comparative biodistribution test, and the significance was evaluated with Student's t-test with EXCEL (Microsoft).

Supplementary Material

Refer to Web version on PubMed Central for supplementary material.

Acknowledgements

H.C. and B.C. contributed equally to this work. This work was mainly supported by grants R01CA218659 and R01EB026207 from the National Cancer Institute and National Institute of Biomedical Imaging and Bioengineering. Graphical abstract was originally created by authors through Biorender.

References

1. Cairns RA; Harris IS; Mak TW, Nature Reviews Cancer 2011, 11 (2), 85–95. [PubMed: 21258394]
2. Gorrini C; Harris IS; Mak TW, Nature reviews Drug discovery 2013, 12 (12), 931–947. [PubMed: 24287781]
3. Nogueira V; Park Y; Chen C-C; Xu P-Z; Chen M-L; Tonic I; Unterman T; Hay N, Cancer cell 2008, 14 (6), 458–470. [PubMed: 19061837]
4. Dolmans DE; Fukumura D; Jain RK, Nature reviews cancer 2003, 3 (5), 380–387. [PubMed: 12724736]
5. Holley AK; Miao L; St. Clair DK; St. Clair WH, Antioxidants & redox signaling 2014, 20 (10), 1567–1589. [PubMed: 24094070]
6. Xu X; Saw PE; Tao W; Li Y; Ji X; Bhasin S; Liu Y; Ayyash D; Rasmussen J; Huo M, Advanced Materials 2017, 29 (33), 1700141.
7. Jin H; Zhu T; Huang X; Sun M; Li H; Zhu X; Liu M; Xie Y; Huang W; Yan D, Biomaterials 2019, 211, 68–80. [PubMed: 31096162]
8. Napoli A; Valentini M; Tirelli N; Müller M; Hubbell JA, Nature materials 2004, 3 (3), 183–189. [PubMed: 14991021]
9. Ma N; Li Y; Xu H; Wang Z; Zhang XJJ o. t. A. C. S, 2010, 132 (2), 442–443.
10. Shim MS; Xia Y, Angewandte Chemie 2013, 125 (27), 7064–7067.
11. Li Z; Hu Y; Fu Q; Liu Y; Wang J; Song J; Yang H, Advanced Functional Materials 2020, 30 (3), 1905758. DOI 10.1002/adfm.201905758.
12. Ma B; Xu H; Zhuang W; Wang Y; Li G; Wang Y, ACS Nano 2020, 14 (5), 5862–5873. DOI 10.1021/acsnano.0c01012. [PubMed: 32379416]
13. Tian Y; Zheng J; Tang X; Ren Q; Wang Y; Yang WJP; Characterization PS, 2015, 32 (5), 547–551.
14. Muhammad F; Wang A; Miao L; Wang P; Li Q; Liu J; Du J; Zhu GJL, 2015, 31 (1), 514–521.
15. Cho S; Park W; Kim H; Jokisaari JR; Roth EW; Lee S; Klie RF; Lee B; Kim D-H, ACS applied nano materials 2018, 1 (9), 4602–4611. [PubMed: 34056557]
16. Cho S; Lee B; Park W; Huang X; Kim D-H, ACS applied materials & interfaces 2018, 10 (33), 27570–27577. [PubMed: 30086228]
17. Kim D-H; Larson AC, Biomaterials 2015, 56, 154–164. [PubMed: 25934288]
18. Choi B; Choi H; Yu B; Kim D-H, ACS nano 2020, 14 (10), 13115–13126. [PubMed: 32885958]
19. Jang H; Min D-H, ACS Nano 2015, 9 (3), 2696–2703. DOI 10.1021/nn506492s. [PubMed: 25560916]
20. Jang H; Kim Y-K; Huh H; Min D-H, ACS Nano 2014, 8 (1), 467–475. DOI 10.1021/nn404833b. [PubMed: 24383549]
21. Abdal Dayem A; Hossain MK; Lee SB; Kim K; Saha SK; Yang G-M; Choi HY; Cho S-G, International journal of molecular sciences 2017, 18 (1), 120.
22. Balfourier A; Luciani N; Wang G; Lelong G; Ersen O; Khelfa A; Alloyeau D; Gazeau F; Carn F, Proceedings of the National Academy of Sciences 2020, 117 (1), 103–113.

23. Nowicka AM; Hasse U; Hermes M; Scholz F, Angewandte Chemie 2010, 122 (6), 1079–1081.
24. Pollock JD; Williams DA; Gifford MA; Li LL; Du X; Fisherman J; Orkin SH; Doerschuk CM; Dinauer MC, Nature genetics 1995, 9 (2), 202–209. [PubMed: 7719350]
25. Decoursey T; Ligeti E, Cellular and Molecular Life Sciences CMLS 2005, 62 (19), 2173–2193. [PubMed: 16132232]
26. Sahay G; Alakhova DY; Kabanov AV, Journal of controlled release 2010, 145 (3), 182–195. [PubMed: 20226220]
27. Lambeth JD; Neish AS, Annual Review of Pathology: Mechanisms of Disease 2014, 9, 119–145.
28. Manke A; Wang L; Rojanasakul Y, BioMed research international 2013, 2013.
29. Tomankova K; Horakova J; Harvanova M; Malina L; Soukupova J; Hradilova S; Kejlova K; Malohlava J; Licman L; Dvorakova M, Food and Chemical Toxicology 2015, 82, 106–115. [PubMed: 25846500]
30. Sykes EA; Dai Q; Sarsons CD; Chen J; Rocheleau JV; Hwang DM; Zheng G; Cramb DT; Rinker KD; Chan WC, Proceedings of the National Academy of Sciences 2016, 113 (9), E1142–E1151.
31. Park W; Park S-J; Cho S; Shin H; Jung Y-S; Lee B; Na K; Kim D-H, Journal of the American Chemical Society 2016, 138 (34), 10734–10737. [PubMed: 27535204]
32. Park W; Cho S; Han J; Shin H; Na K; Lee B; Kim D-H, Biomaterials Science 2018, 6 (1), 79–90. DOI 10.1039/C7BM00872D.
33. Tsoi KM; MacParland SA; Ma X-Z; Spetzler VN; Echeverri J; Ouyang B; Fadel SM; Sykes EA; Goldaracena N; Kaths JM, Nature materials 2016, 15 (11), 1212–1221. [PubMed: 27525571]
34. Poon W; Zhang Y-N; Ouyang B; Kingston BR; Wu JL; Wilhelm S; Chan WC, Acs Nano 2019, 13 (5), 5785–5798. [PubMed: 30990673]
35. Sadauskas E; Danscher G; Stoltenberg M; Vogel U; Larsen A; Wallin H, Nanomedicine: Nanotechnology, Biology and Medicine 2009, 5 (2), 162–169. DOI 10.1016/j.nano.2008.11.002. [PubMed: 19217434]
36. Kolosnjaj-Tabi J; Javed Y; Lartigue L; Volatron J; Elgrabli D; Marangon I; Pugliese G; Caron B; Figuerola A; Luciani N; Pellegrino T; Alloyeau D; Gazeau F, ACS Nano 2015, 9 (8), 7925–7939. DOI 10.1021/acsnano.5b00042. [PubMed: 26168364]

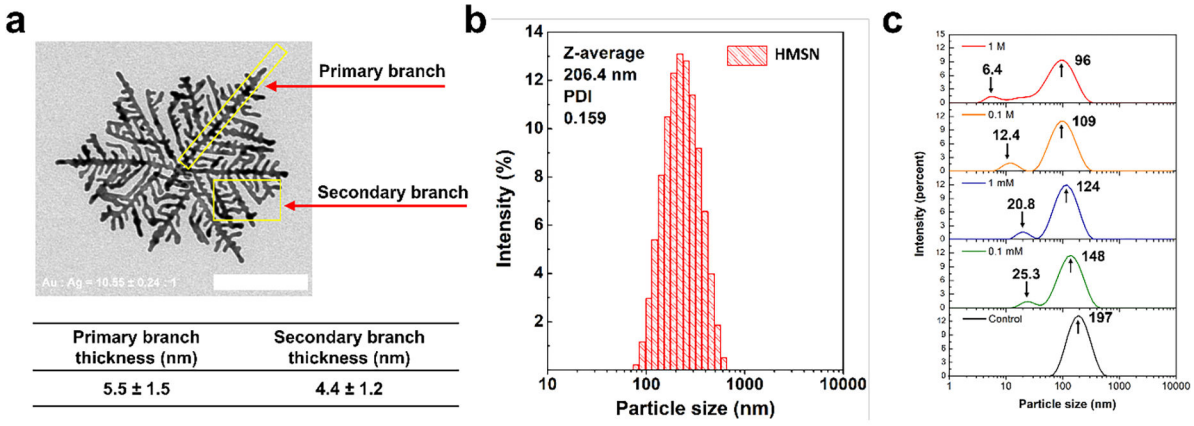

Primary branch thickness (nm)	Secondary branch thickness (nm)
5.5 ± 1.5	4.4 ± 1.2

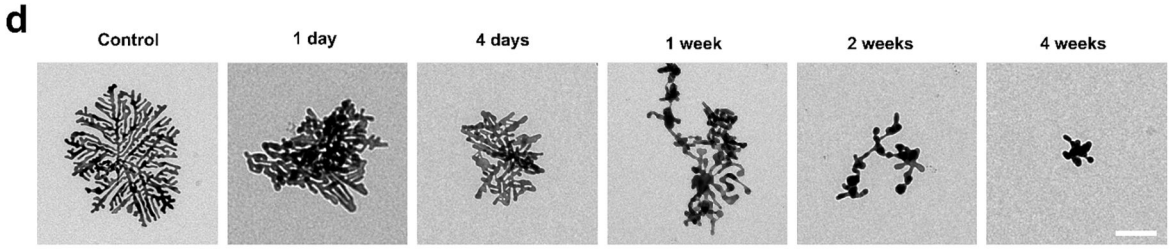

e

Treatment type	HMSN H_2O_2 (0.1 M)	
	Size (nm)	PDI
Control	206	0.157
1 day	166	0.223
4 days	134	0.298
7 days	128	0.302
14 days	118	0.368
28 days	77	0.468

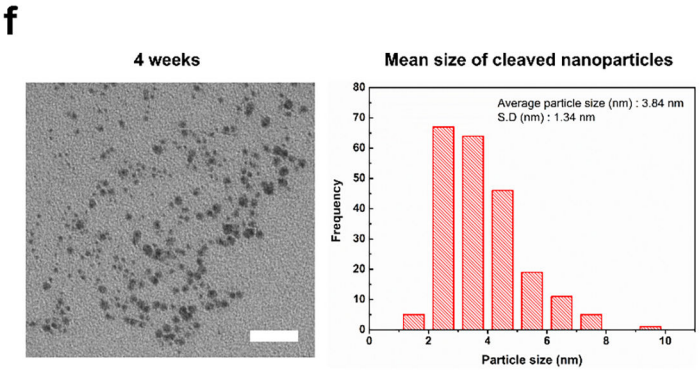

Figure 1.

a) Representative transmission electron microscopic image of HMSN (the size bar represents 100 nm) and structural information of HMSN based on observation by TEM. **b)** Mean particle size and distribution of HMSN obtained from dynamic light scattering (DLS). **c)** Size and distribution measurement using DLS after the incubation of HMSN with various concentration of H_2O_2 (0, 0.1 mM, 1 mM, 0.1, and 1 M), **d)** Representative TEM images of HMSN samples collected at the predetermined incubation time (1 day, 4 days, 1 week, 2 weeks, and 4 weeks) with H_2O_2 (the size bar represents 100 nm). **e)** A table showing particle size changes on the HMSN by treatment of H_2O_2 after predetermined time. **f)** TEM images of small nanoparticles generated from HMSN after the incubation with H_2O_2 (the size bar represents 100 nm) and size information of small nanoparticles derived from HMSN based on more than 200 nanoparticles counted from TEM images.

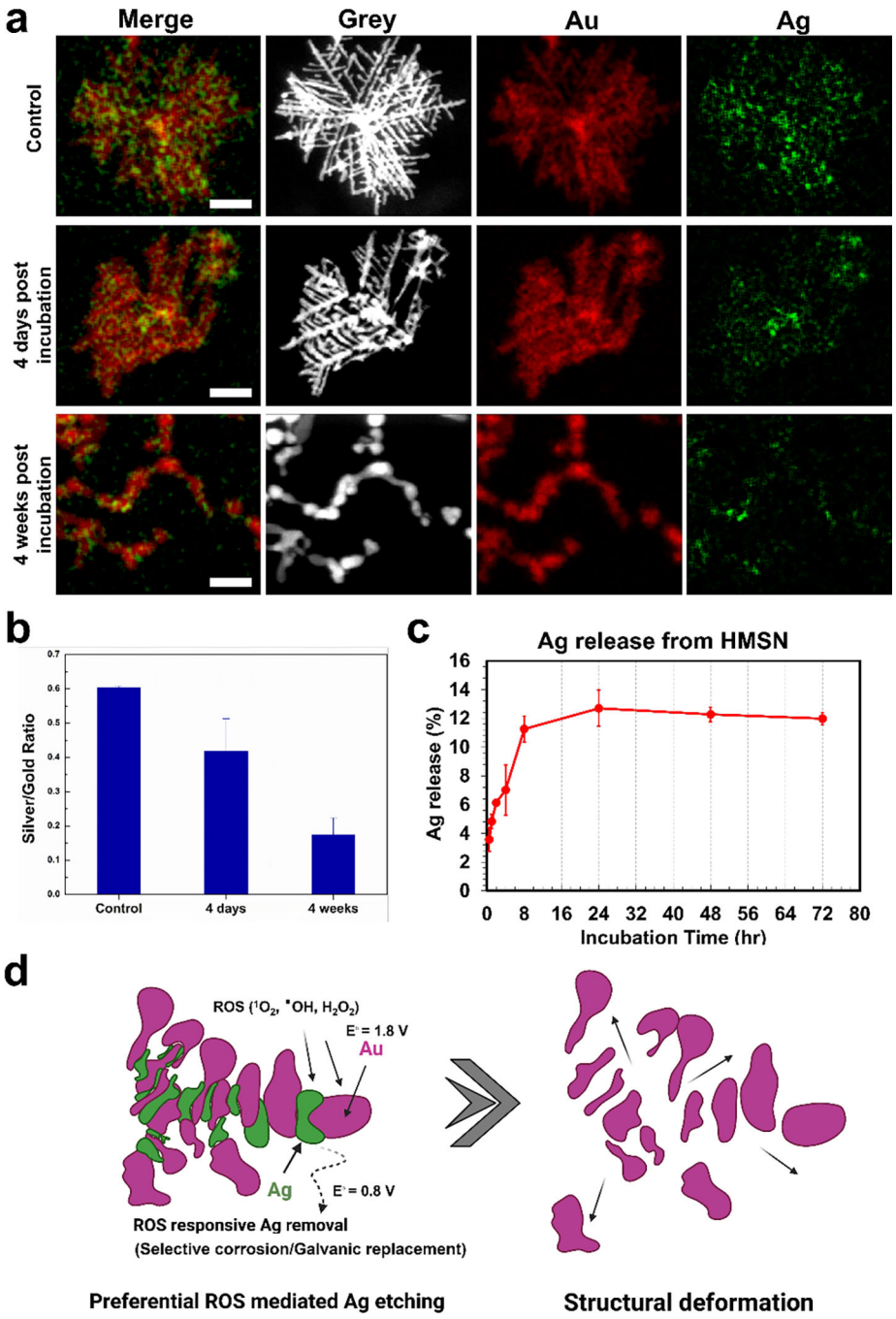

Figure 2.

a) Scanning transmission electron microscope (STEM) images of HMSN after the incubation with H_2O_2 (gold and silver in images were colored with red and green color, respectively and the size bar represents 100 nm). **b)** A graph of the silver to gold ratio calculated from the ROI quantification of each element. **c)** Quantification of silver element released from HMSN by H_2O_2 up to 72 hours. **d)** A schematic image of the cleavage mechanism of HMSN in the presence of ROS.

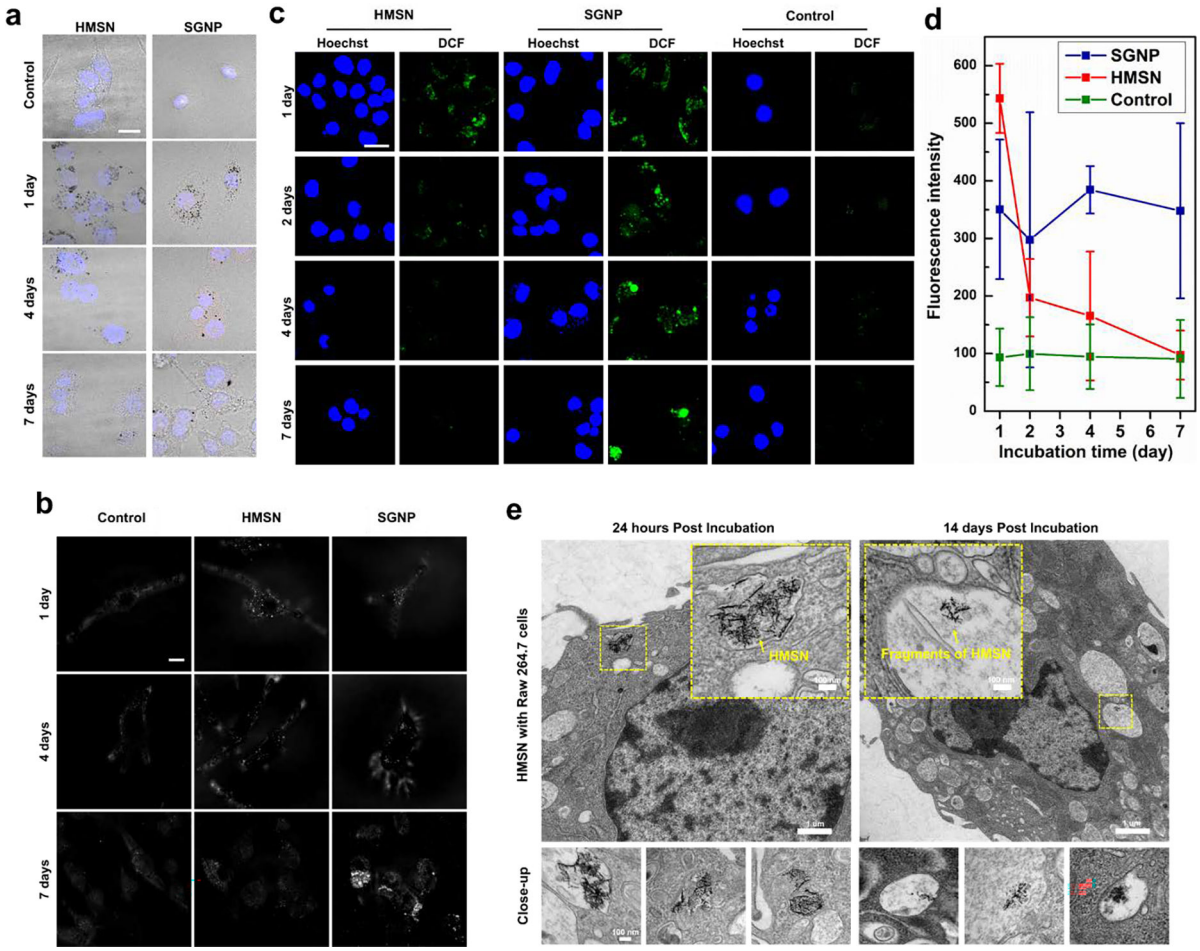

Figure 3.

a) Bright field images merged with DAPI signals of cells using confocal microscopy (black dots indicate the gold nanoparticles accumulated in cells). **b)** Confocal reflective microscopic images for the detection of gold nanoparticle in living cell after uptake of gold nanoparticles (HMSN and SGNP). **c)** Confocal laser scanning microscopic images for ROS quantification in live cells after uptake of gold nanoparticles (HMSN and SGNP). **d)** Quantification of green fluorescence (DCF2-DA) for measuring ROS generation of RAW 264.7 cells after predetermined time up to 7 days. **e)** Cell TEM images of RAW 264.7 macrophage cells co-incubated with HMSN. The images at bottom line were obtained from cell samples on same TEM grid from cells.

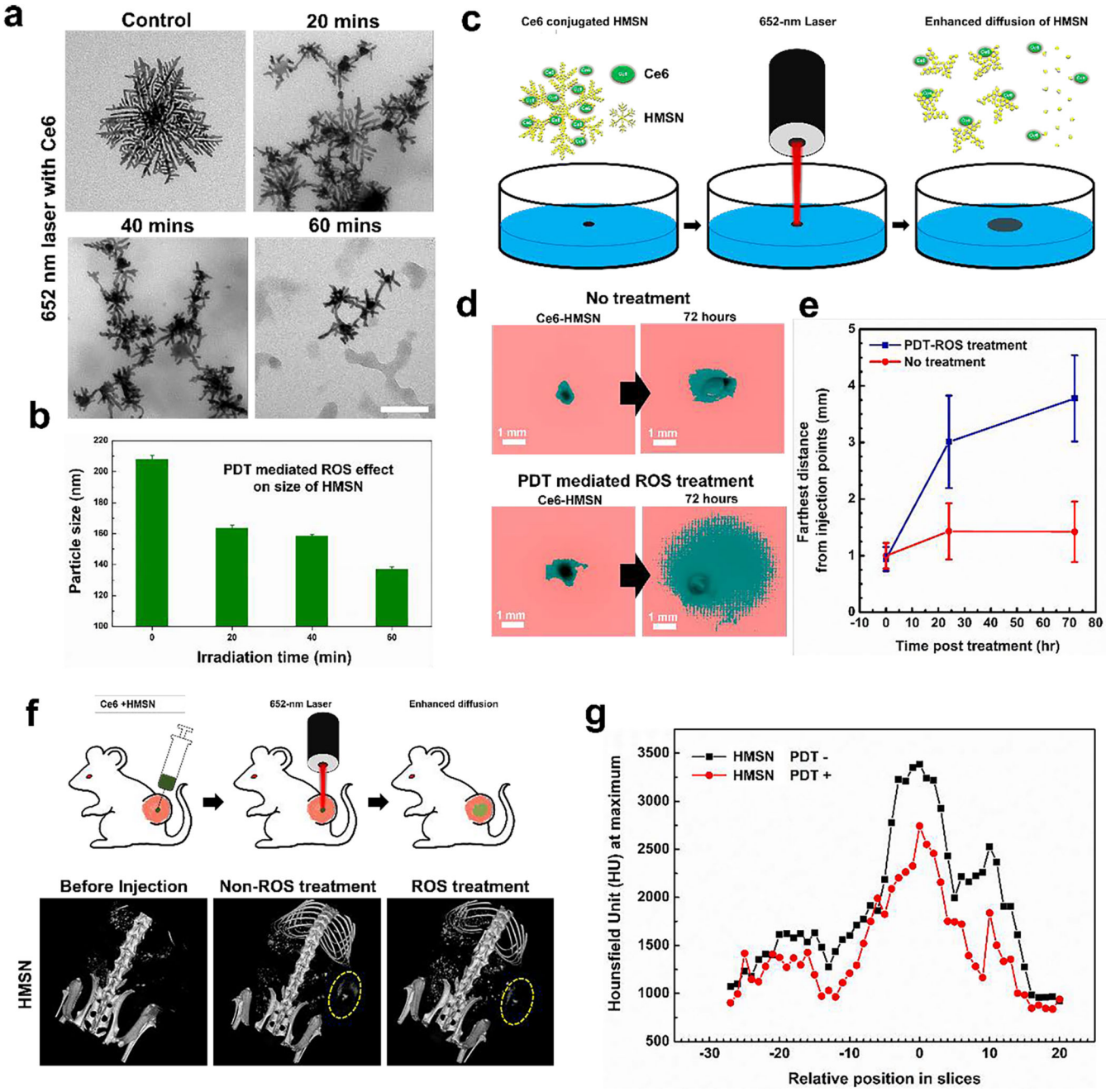

Figure 4.

a. TEM images of HMSN loaded with Ce6 after the various irradiation doses by varying the exposure time (20, 40, and 60 min with 652 nm laser (120 mW/cm^2). **b.** Measurement of hydrodynamic size after the treatment of 652-nm laser using DLS. **c.** A schematic image introducing experimental set-up for evaluating the diffusion of nanoparticles after ROS treatment. **d.** Images taken by a digital camera before/after inducing ROS after applying threshold function for determining the diffused distance of nanoparticles in tissue mimicking agarose hydrogel. **e.** A measurement of the distance that HMSN traveled from the seeded point after the induction of ROS or not. **f.** Observation of contrast effect of gold

nanoparticles (HMSN and SGNP) by computed tomographic images of tumor bearing mice treated with gold nanoparticles (HMSN and SGNP) and ROS inducing laser subsequently. **g**. A comparison of CT contrast effect (maximum value in ROI of each CT slices) of HMSN before and after treatment of ROS in tumor.

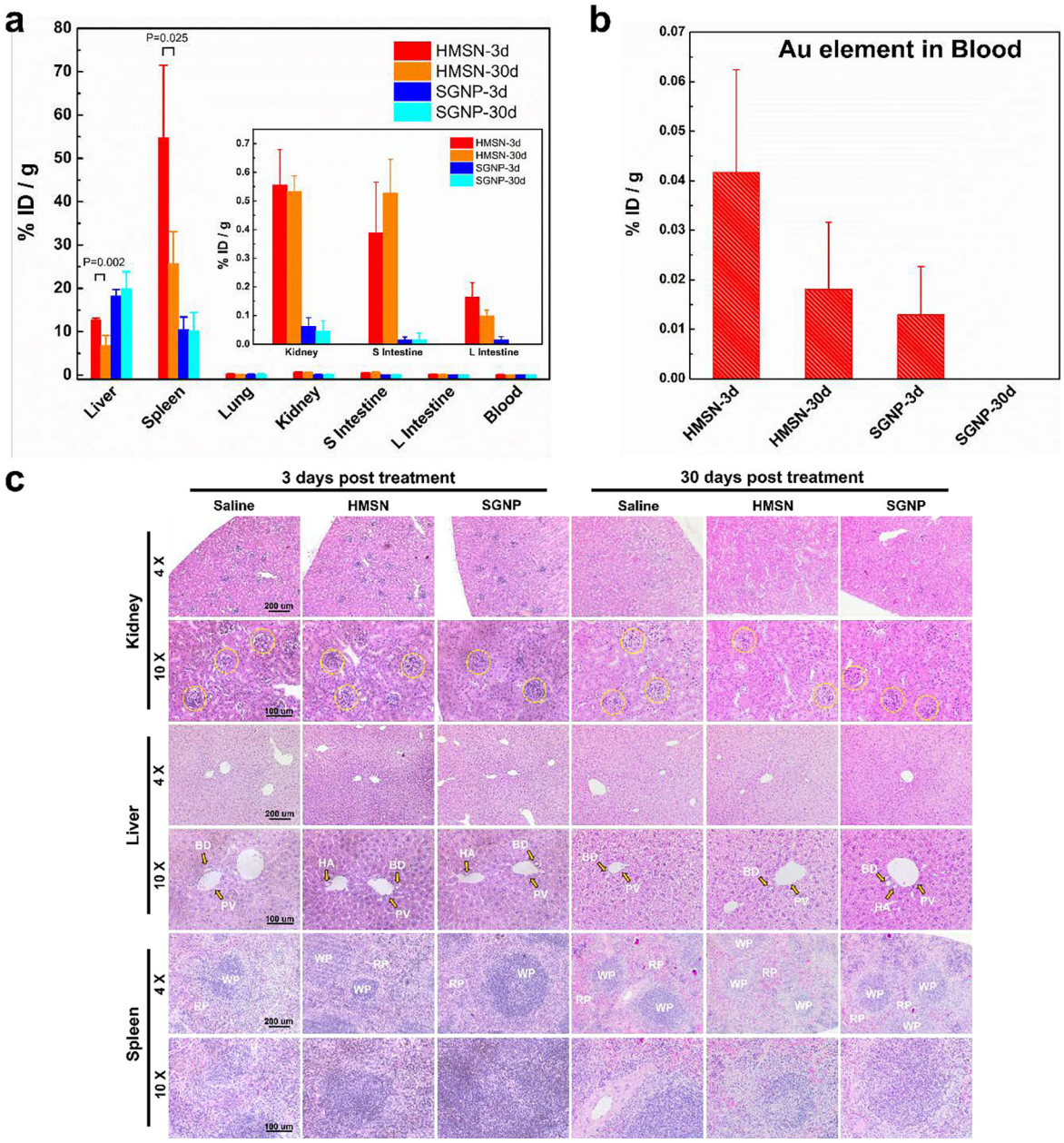

Figure 5.

a) Comparative study of biodistribution profiles of gold nanoparticles (HMSN and SGNP) after 3 days and 30 days post injection. (Statistical analysis was performed with Student's T-test and 5 mice per each group were examined.) **b)** Elemental (Au) quantification in blood of each group. **c)** Pathological evaluation of HMSN on excretory organs (kidney, liver, and spleen) by hematoxylin-eosin staining. Yellow dotted circle in the images of kidney samples indicates glomerulus (GM). the portal veins (PV), bile ducts (BD), hepatic arteries (HA) were annotated with yellow arrows on the liver samples. The area of white pulp (WP) and red pulp (RP) was highlighted on the spleen sections.